hydrogen

MDPI

Article

Composition-Tunable Power-to-Syngas: Techno-Economic and Sustainability Assessment

Asmae Abousalmia and Seckin Karagoz *

Department of Chemical Engineering, College of Engineering, Qatar University, Doha P.O. Box 2713, Qatar; aa2004971@student.qu.edu.qa

* Correspondence: skaragoz@qu.edu.qa

Abstract

This study investigates a composition-tunable power-to-syngas platform in which a natural-gas-fired Allam–Fetvedt (AF) supercritical CO_2 (sCO_2) power cycle is coupled with three electrolysis architectures for converting internally available CO_2 and H_2O into synthesis gas. Because the AF power block is fueled by natural gas, the integrated system is treated here as a low-carbon process-integration concept rather than as a fully renewable energy pathway. Three Aspen HYSYS configurations are evaluated on the same 437 MW-net AF power basis: (i) separate PEM water electrolysis and AEM CO_2 electrolysis followed by H_2/CO blending, (ii) AEM co-electrolysis, and (iii) high-temperature solid-oxide co-electrolysis. The H_2/CO molar ratio is varied from 0.25 to 2.0. Increasing H_2/CO lowers the mass of syngas produced per unit electrical input while increasing stoichiometric water demand and oxygen generation; lower H_2/CO ratios require greater CO_2 conversion. The 5.07×10^6 kg h^{-1} CO_2 value used in the process model represents the internal circulating sCO_2 inventory rather than net carbon generation. On the common AF basis, only a controlled fraction of the net CO_2-rich product stream is routed to syngas synthesis, while the remainder is retained for recycling or export/storage. The electrolysis section requires approximately 8.9–35% of the recovered AF process-water stream on a stoichiometric basis, and the oxygen co-product is equivalent to approximately 22.9–26% of the AF oxygen requirement. These resource-integration quantities are reported without crediting additional electrical power to the electrolyzers. The sustainability results are relative process-level screening scores and do not constitute a cradle-to-gate life-cycle assessment. Under the adopted economic assumptions, positive returns are concentrated mainly at H_2/CO ≈ 1.5–2.0 for low-temperature configurations, whereas the solid-oxide route remains strongly constrained by current capital and replacement costs. Overall, the preferred operating region depends jointly on electrolysis architecture, syngas composition, and the economic boundary used for valuation.

Keywords: power-to-syngas; tunable H_2/CO ratio; CO_2 utilization; Allam–Fetvedt cycle; co-electrolysis; process integration; techno-economics

Academic Editor: Jean St-Pierre

Received: 27 September 2026
Revised: 3 November 2026
Accepted: 4 November 2026
Published: 5 November 2026

Copyright: © 2026 by the authors. Licensee MDPI, Basel, Switzerland. This article is an open access article distributed under the terms and conditions of the Creative Commons Attribution (CC BY) license.

1. Introduction

Syngas is a central intermediate for the manufacture of fuels and chemicals, including methanol, dimethyl ether, Fischer–Tropsch liquids, oxo-alcohols, acetic-acid derivatives, and other carbonyl products [1–3]. It is conventionally produced by steam reforming, partial oxidation, autothermal reforming, or gasification of carbon-containing

feedstocks, so its production route strongly influences energy demand and carbon intensity [1,2]. In addition to the production pathway, the H_2/CO molar ratio is a key product specification because different downstream chemistries require different hydrogen-to-carbon-monoxide balances. CO-rich mixtures are used in carbonylation-related applications, oxo-synthesis commonly operates around approximately equimolar H_2/CO feeds, and methanol/DME/Fischer–Tropsch applications generally require progressively more hydrogen-rich syngas, depending on the downstream reactor chemistry and any upstream conditioning [1–3]. This composition dependence motivates treating H_2/CO not as a fixed product property but as a process-design variable. As can be seen in Figure 1, global demand for syngas and syngas-derived products remains substantial and is expected to grow with continued demand for chemicals, fuels, and lower-carbon feedstocks [3,4].

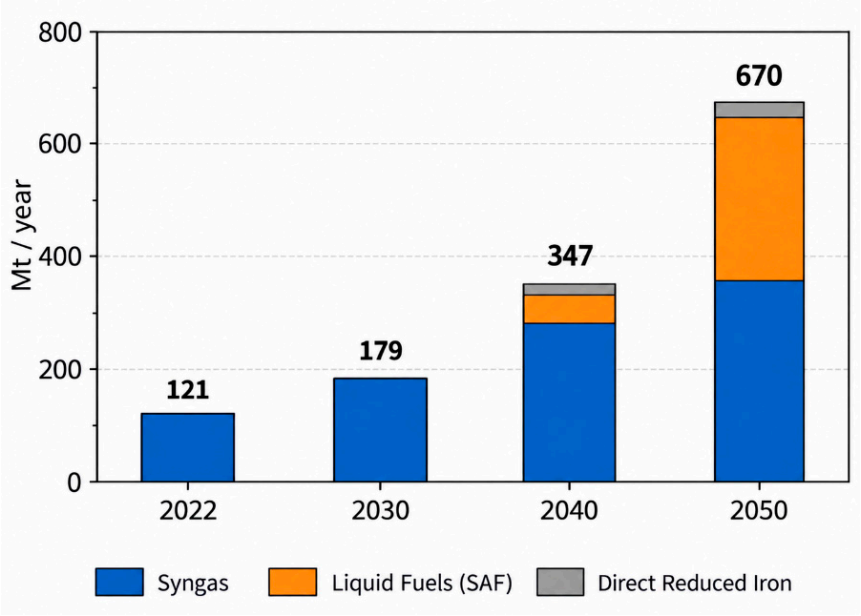


Figure 1. Long-term prediction of the syngas market size [3].

Traditionally, syngas has been produced in large, centralized facilities to leverage economies of scale, a model that carries negative environmental impacts due to fossil-based feedstocks, energy-intensive operations, associated greenhouse-gas and pollutant emissions, and risks from long-distance transport [5]. Advancing new technologies and improving existing processes in line with sustainability criteria is essential for delivering cleaner and more affordable energy while avoiding additional economic and energetic penalties [6]. Yet designing genuinely sustainable industrial processes remains a major and ongoing challenge for the chemical sector at the global scale [7]. Embedding sustainability considerations directly into the process design helps move toward this goal by preventing or reducing negative impacts, but robustly quantifying sustainability performance and using those results to support sound decision-making is both critical and non-trivial [7,8]. Accordingly, there is a clear need for a structured methodological framework that can capture and abstract complex process behavior while at the same time providing transparent analysis and communication through well-chosen sustainability indicators [9].

Electrochemical routes provide an alternative way to produce the H_2 and CO components of syngas by converting H_2O and CO_2 using electricity. When the electricity is renewable, such routes can support renewable or green products which when electricity is supplied by a fossil-fueled process with integrated carbon capture, the more appropriate description is low-carbon electrochemical production. Water electrolysis is already deployed commercially for hydrogen production, whereas CO_2 electrolysis and CO_2/H_2O co-

electrolysis remain at lower levels of technological maturity and are being developed across low- and high-temperature platforms [3–5,10]. Their main process-level advantages are modularity, controllable product composition, compatibility with electrified process integration, and the possibility of coupling with concentrated CO_2 streams. These benefits do not eliminate the need to account for stack efficiency, faradaic selectivity, auxiliary power, gas conditioning, and durability when moving from conceptual flowsheets to industrial implementation.

The Allam–Fetvedt (AF) cycle is an oxy-combustion sCO_2 Brayton power cycle that produces dispatchable electricity while generating a concentrated, high-pressure CO_2-rich stream that can be captured without a conventional post-combustion separation train [11–13]. In the present study, the AF cycle is fueled by natural gas; therefore, its electricity is classified as low-carbon within the modeled process boundary. The value of the AF platform for this work is its process integration: it supplies net electricity, recovered water, and a concentrated CO_2 stream that can be directed to electrochemical conversion. Electrolyzer-generated O_2 can also be returned to the oxy-combustion section as a partial material substitute for externally supplied oxygen. Importantly, the present analysis distinguishes these process-integration benefits from full life-cycle environmental performance. Upstream natural-gas production and methane leakage, oxygen-production infrastructure, electrolyzer manufacturing and replacement, and downstream syngas conversion are outside the operational boundary and require separate life-cycle assessments.

Recent studies have increasingly explored the integration of supercritical-CO_2 power cycles, electrolysis, carbon utilization, and synthetic-fuel production. Gai et al. developed a near-zero-carbon-emission power concept in which CO_2 and H_2O produced during fuel conversion were recycled to electrochemical synthesis routes, demonstrating the potential role of CO_2 and H_2O as internally integrated feedstocks for renewable-energy storage and synthetic-fuel production [14]. Zhang et al. subsequently proposed a biomass-to-methanol system integrating water electrolysis with a supercritical CO_2 power cycle, in which electrolytic hydrogen supports methanol production while waste heat is recovered through the sCO_2 cycle [15]. Although these systems differ from the Allam–Fetvedt architecture adopted here, they illustrate the wider process-integration potential of combining electrolysis, carbon utilization, fuel synthesis, and sCO_2-based power generation.

Allam-cycle-specific studies have also begun extending the cycle beyond conventional natural-gas-fired electricity production. Candelaresi and Spazzafumo integrated an Allam-cycle power unit with biomass-derived substitute-natural-gas production, electrolysis, methanation, and CCUS, demonstrating the potential for power-to-gas integration and internal utilization of electrolysis-derived oxygen [16]. More recently, Manente et al. investigated a methanol-fired Allam cycle based on synthetic e-methanol produced from CO_2 hydrogenation with electrolytic hydrogen. Their configuration uses electrolysis-derived oxygen for oxy-combustion, recovers condensed water for electrolysis, and distributes CO_2 between recycling and methanol synthesis, thereby illustrating a highly integrated Allam–electrolysis–e-fuel architecture [17]. These developments confirm the growing interest in exploiting the distinctive CO_2, H_2O, O_2, heat, and power interfaces of the Allam cycle for power-to-X applications. The present study advances this direction by focusing specifically on composition-tunable syngas rather than a fixed downstream fuel and by comparing separate PEM + AEM production, low-temperature AEM co-electrolysis, and high-temperature SOE co-electrolysis over a common H_2/CO design window.

The study has four objectives: (i) define three AF-integrated routes capable of producing tunable H_2/CO syngas; (ii) quantify composition-dependent syngas productivity, CO_2 conversion demand, water use, and oxygen recovery on a common 437 MW-net basis; (iii) examine how material, energy, and environmental sustainability change across the composition window; and (iv) identify the H_2/CO ranges for which the integrated

configurations become economically attractive under the adopted 25-year CAPEX/OPEX and product-value assumptions. Detailed AF-cycle modeling, cell-level Aspen HYSYS flowsheets, indicator definitions, and costing tables are provided in the Supplementary Materialss so that the main manuscript remains centered on syngas design decisions.

The present manuscript is a direct continuation and extension of the previously published study by Abousalmia and Karagoz (2026) [18], which focused on the sustainability and techno-economic assessment of hydrogen production using low- and high-temperature water electrolysis. In contrast, the current work extends the same overall methodological framework toward syngas production, with emphasis on the performance and sustainability implications of the corresponding integrated process configurations. To avoid unnecessary duplication of material that has already been published and validated in the earlier work, detailed descriptions of the common process background, methodological foundations, sustainability framework, economic assumptions, and calculation procedures are not repeated extensively in the main text. Instead, these materials are provided in the Supplementary Materials, while the main manuscript focuses on the new process configuration, syngas-related results, comparative analysis, and the additional scientific insights arising from this extension. The previously published study should therefore be regarded as the methodological foundation of the current work, whereas the present manuscript specifically addresses the new syngas-production case and its associated technical, environmental, and economic performance.

Compared with the previously published power-to-hydrogen study [18], which evaluated AF-integrated PEM, AEM, and SOE water-electrolysis pathways for hydrogen production under a common 437 MW-net power basis, the present work represents a substantial extension from single-product hydrogen generation to a composition-tunable power-to-syngas platform. The earlier study established the integrated Allam–Fetvedt/electrolysis framework and assessed hydrogen production using process simulation, techno-economic analysis, and multidimensional sustainability indicators. In contrast, the current study introduces three distinct syngas-production architectures—separate PEM water electrolysis plus AEM CO_2 electrolysis with downstream blending, AEM co-electrolysis, and high-temperature SOE co-electrolysis—and evaluates them over a wide H_2/CO molar-ratio range of 0.25–2.0. The main novelty therefore lies not simply in applying the previous framework to another product but in explicitly coupling electrolysis architecture, CO_2 utilization, syngas composition, water demand, oxygen recovery, energy integration, sustainability, and project economics within the same process boundary. This composition-dependent analysis reveals trade-offs that do not arise in hydrogen-only production, particularly the decrease in syngas productivity with increasing H_2/CO ratio, the shift between CO_2 and H_2O utilization, and the emergence of composition-specific economic operating windows. Accordingly, the present study advances the earlier hydrogen-focused work toward a broader power-to-molecules concept in which captured CO_2 and internally recovered water are converted into tunable syngas suitable for different downstream chemical and fuel synthesis pathways, while avoiding unnecessary repetition of the previously established AF-cycle and sustainability methodology.

2. System Configuration and Syngas Design Space

Figure 2 summarizes the integrated process and should be read as the system-boundary definition for the present analysis. The AF power block supplies net electricity, a concentrated CO_2-rich stream, and recovered process water to a syngas-production section. The AF system is operated at the same simulated scale for every case, and its 437 MW-net electrical output defines the fixed power budget used to compare the three electrolysis architectures without changing plant scale.

Within the syngas section, the electrical power is distributed according to the selected architecture and target H_2/CO ratio. The produced H_2 and CO are combined where required, while oxygen is collected as a co-product to be partially recycled into the AF oxy-combustion system. Figure 2 summarizes the process interface; detailed AF-cycle equipment and stream data are reported in Supplementary Section S1.

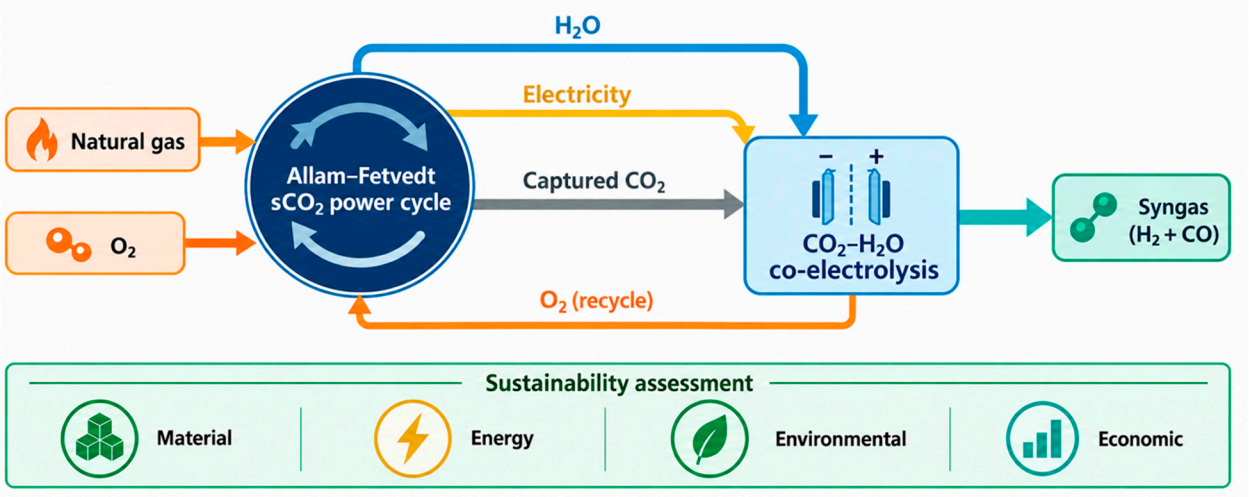


Figure 2. Integrated AF-to-syngas process concept and internal resource exchanges.

The process boundary is designed to minimize direct CO_2 release by retaining the bulk of the carbon inventory inside the AF recycle loop and converting only a controlled side stream to CO-containing syngas. The resulting claim is therefore limited to the modeled steady-state process boundary; upstream natural-gas supply and downstream syngas conversion are outside the present analysis.

The distinguishing operating variable is the product H_2/CO molar ratio. Adjusting the relative contribution of water electrolysis and CO_2 reduction changes the syngas composition from CO-rich (H_2/CO = 0.25) to hydrogen-rich (H_2/CO = 2.0). This provides a direct link between product specification and process resource demand.

2.1. Allam–Fetvedt Interface and Fixed-Power Basis

The AF cycle is used as the common upstream platform rather than as the main object of comparison. Under the adopted Aspen HYSYS conditions, it delivers 795 MW gross and 437 MW-net power. The 437 MW value is the net output of the baseline AF model after the internal and auxiliary requirements already included in that model. It is therefore used as a fixed comparison basis for electrolysis. The oxygen co-product from electrolysis is not converted into additional electrical power and added to the 437 MW budget; it is treated only as a potential material/economic offset to external oxygen supply. Likewise, the present model does not separately resolve every downstream electrolysis auxiliary, such as final product compression, polishing, or detailed gas-separation power. These omissions are explicitly retained as limitations of the system-level comparison. The AF model also generates an internal water stream and a concentrated CO_2-rich product stream, while a much larger sCO_2 inventory circulates internally as working fluid. Detailed thermodynamic assumptions and stream conditions are provided in the Supplementary Materials, Section S2, and in the preceding AF study [18].

2.2. Electrolysis Architectures for Tunable Syngas

Three architectures (Figure 3) are compared because they achieve composition control in fundamentally different ways: independent generation and blending of H_2 and CO,

low-temperature co-electrolysis, and high-temperature co-electrolysis. PEM, AEM, and solid-oxide technologies are used as representative low- and high-temperature platforms. Their detailed cell-level operating assumptions and Aspen implementations are documented in Supplementary Section S3; the main text focuses on the architectural consequences for tunable syngas production.

Design 1 separates the two electrochemical functions. A PEM unit produces H_2 from H_2O, an AEM unit produces CO from CO_2, and the two product streams are blended to the target H_2/CO ratio. Because H_2 and CO are independently generated, this configuration provides direct composition control but requires two electrolysis trains. Design 2 uses a single AEM co-electrolysis train in which the competition between CO_2 reduction and hydrogen evolution determines the H_2/CO ratio. This architecture is simpler than Design 1 but couples product composition more strongly to electrode selectivity and operating conditions. Design 3 uses solid-oxide co-electrolysis at elevated temperature. Part of the splitting energy can be supplied as heat, creating stronger thermal-integration potential with the AF cycle. The advantage is offset by the more demanding high-temperature materials, sealing, and replacement requirements reflected in the economic analysis.

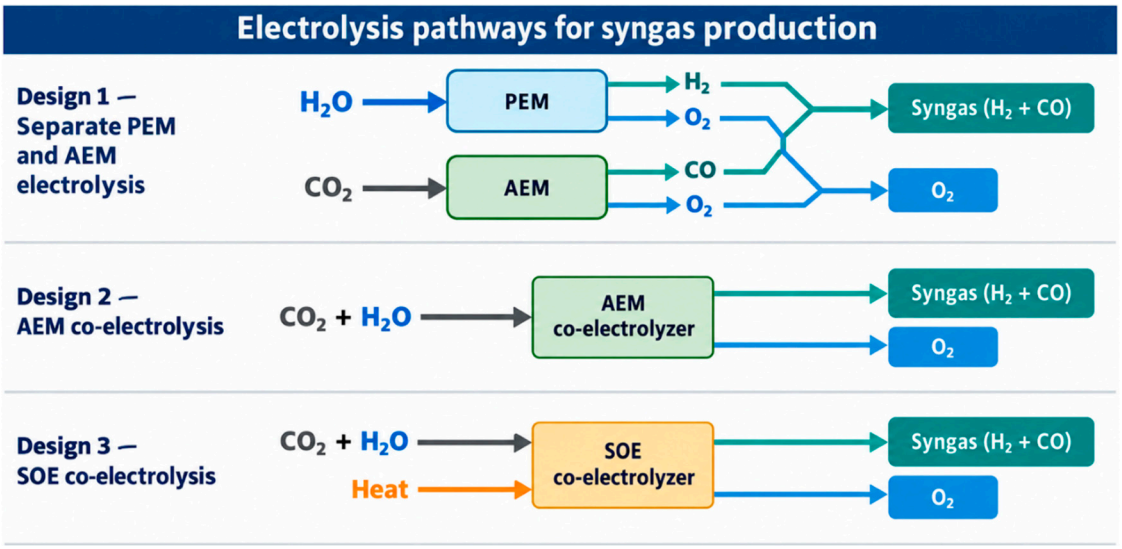


Figure 3. Illustration of the three different syngas-production scenarios analyzed in this study.

3. Modeling Framework

3.1. Power Matching and Process Boundary

All configurations are constrained by the same 437 MW-net electrical output from the AF block. The electrolysis system is therefore scaled until its total electrical demand matches the available AF power, while the associated CO_2 and H_2O feeds and O_2 co-product are calculated consistently from the selected reactions and target H_2/CO ratio. This fixed-power basis separates the effect of electrolysis architecture and product composition from simple capacity differences.

$$P_{\text{Allam,net}} = P_{\text{elec,tot}} \quad (1)$$

where

$P_{\text{Allam,net}}$ = net electrical power produced by the Allam–Fetvedt cycle;
P_{electot} = total electrical power consumed by the electrolyzers' system.

3.2. Electrolyzer Models and H_2/CO Control

The three configurations are evaluated over H_2/CO ratios from 0.25 to 2.0 using the same AF power budget. For each target composition, the required contributions of H_2O

electrolysis and CO_2 conversion are determined, the equivalent electrolysis capacity is scaled from the Aspen HYSYS single-cell process blocks, and the corresponding syngas, oxygen, carbon dioxide, and water flows are calculated. The conversion reactors and component splitters are process-level surrogates used to close stoichiometric mass and energy balances; they are not electrochemical polarization models and should not be interpreted as demonstrating near-100% single-pass faradaic conversion in an industrial stack. The overall technology efficiencies used for scale-up represent the literature-based process efficiencies and therefore constrain the plant-level power demand even when the stoichiometric conversion block is written as complete conversion. The detailed single-cell flowsheets and sample stream tables for $H_2/CO = 1$ are provided in the Supplementary Materials, Section S4.

The energy-matching relation can be generalized by writing the total electrolyzers' system power demand as a double sum over the technology type (i) and electrolysis mode (j):

$$P_{elec,tot} = \sum_i \sum_j P_{cell,req}^{(i,j)} = \sum_i \sum_j N_{cell}^{(i,j)} \frac{P_{cell,spec}^{(i,j)}}{\eta_{cell}^{(i,j)}} \quad (2)$$

where

i = electrolyzer technology type, i = SOE,PEM,AEM;

j = electrolysis feed type, j = H_2O or CO_2 or $CO_2 + H_2O$;

$P_{\mathrm{elec,tot}}$ = total electrical power allocated to all electrolyzers (kW);

$P_{\mathrm{cell,req}}^{(i,j)}$ = total electrical power required by single electrolyzer cell of type (i,j) (kW);

$N_{\mathrm{cell}}^{(i,j)}$ = number of cells of technology i operating in mode j;

$P_{\mathrm{cell,spec}}^{(i,j)}$ = single-cell electrical power consumption for type i and mode j, obtained from Aspen HYSYS (kW per cell at the chosen operating point);

$\eta_{\mathrm{cell}}^{(i,j)}$ = electrical efficiency (0–1) of a single cell of type i and mode j.

The Aspen models represent the reaction stoichiometry using conversion reactors and component splitters at selected process conditions. Design 1 models PEM water electrolysis and AEM CO_2 electrolysis separately before product blending; Design 2 represents low-temperature CO_2–H_2O co-electrolysis; and Design 3 represents the corresponding high-temperature solid-oxide route. This modeling choice is appropriate for a plant-level comparative mass/energy balance, but it does not resolve electrode kinetics, polarization losses, membrane transport, catalyst selectivity, degradation, or transient operation. Consequently, the study is interpreted as a theoretical process-integration and screening analysis rather than as experimental validation of individual electrolyzer stacks.

Validation Basis and Composition-Control Assumptions

Model validation was carried out at the level appropriate to the system model. The AF block delivers an overall net efficiency of approximately 55%, consistent with the practical 55–57% range discussed for realistic Allam–Fetvedt operation in the literature [13,18]. For the electrolysis section, the process efficiencies and operating characteristics were selected from literature-based ranges and from the previously published AF-electrolysis study [18]. The comparison therefore uses externally supported technology-level efficiencies rather than claiming that the simplified HYSYS conversion reactors reproduce stack polarization curves or faradaic efficiencies.

For Design 2, the specified H_2/CO range is treated as a target composition window for system-level scenario analysis. Experimental and review literature confirms that low-temperature CO_2 electrolysis can produce tunable H_2/CO mixtures by changing catalyst, current density, electrolyte/membrane environment, gas feed, and the competition

between CO_2 reduction and hydrogen evolution [2–4,10]. However, the present HYSYS model does not calculate the faradaic-efficiency map, cell voltage, or current-density operating point required to obtain each target ratio. Accordingly, the manuscript no longer interprets every ratio between 0.25 and 2.0 as an experimentally validated operating point of a single AEM stack; instead, these ratios define a process-design envelope whose electrochemical feasibility must be verified in future stack-level experiments or detailed electrochemical models.

Similarly, the 85% SOE efficiency represents a literature-based high-temperature electrolysis assumption. No explicit AF-to-SOE heat exchanger, SOE heat duty, minimum temperature approach, or feedback of extracted heat on AF net power is modeled in the present work. Therefore, no additional numerical heat-recovery credit is applied beyond the adopted technology efficiency. References to heat integration in the results are interpreted as integration potential rather than as a quantified heat-exchanger design result.

3.3. Sustainability Assessment

Methodological sustainability assessment provides a flexible screening framework for evaluating process performance at different scales, from individual equipment to complete flowsheets [6–9,19–22]. The indicator taxonomy and the material, energy, environmental, and economic dimensions used here are based on previously published process-sustainability methodologies, including the Ruiz-Mercado indicator framework and the previously applied AF sustainability methodology [6–9,18]. The normalized scores are therefore relative decision-support metrics; they are not substitutes for absolute life-cycle inventory results or site-specific regulatory metrics.

In this study, the assessment is organized into seven phases: (1) problem/system definition and data collection, (2) technology and option selection, (3) generation of flowsheet alternatives, (4) model and simulation development, (5) selection or development of sustainability indicators, (6) screening of alternatives, and (7) identification of feasible and promising process options. During phase 5, sustainability indicators are selected from the literature or adapted to the specific process and grouped into economic, energy, environmental, and material dimensions. Their selection is critical because they provide the quantitative basis for comparing alternatives. Indicator weights can be determined using expert judgment, stakeholder preferences, AHP, equal weighting, statistical/data-driven methods, or broader MCDA approaches [19–21].

Equal weighting was adopted as a transparent baseline because the objective is comparative screening of the three AF–electrolyzer architectures without assigning a priori preference to one sustainability dimension [19–22]. Each indicator contributes equally after normalization. This choice avoids stakeholder-specific preference bias, but it does not imply that all indicators have equal physical importance in every deployment context. Accordingly, differences in only a few percentage points between alternatives are interpreted cautiously, and the manuscript does not claim that the ranking would necessarily remain unchanged under every alternative weighting scheme.

The normalization procedure maps each indicator onto a 0–100% scale using a best target and a worst-case reference. The reference values in Table 1 were inherited from the methodological sustainability framework used in the preceding process-sustainability studies [6–9,18] and are applied consistently to all alternatives. They should be interpreted as screening anchors rather than universal thermodynamic or regulatory limits. For indicators for which lower values are preferable, the normalization direction is reversed so that 100% always denotes the more desirable result. Because some reference values (for example, mass-intensity and EROI anchors) are method-dependent, the absolute normalized score is sensitive to the selected range. The present study therefore emphasizes cross-design trends under a common normalization basis and avoids treating small differences

in the aggregate scores as statistically or universally robust. Future work should explicitly test alternative ranges and weighting schemes using AHP, entropy weighting, TOPSIS, or stakeholder-specific weights.

The following sustainability scale transforms any indicator score to a dimensionless form, and is used for each indicator:

$$S_{i,j} = \frac{X_{i,j} - X_{i,\min}}{X_{i,\max} - X_{i,\min}} \times 100 \quad (3)$$

where

$S_{i,j}$ = normalized sustainability score of indicator i for alternative j, %;
$X_{i,j}$ = calculated value of indicator i for alternative j;
$X_{i,\min}$ = reference worst-case value of indicator i;
$X_{i,\max}$ = reference best-case value of indicator i;
i = sustainability indicator index;
j = process-alternative index.

For indicators for which a lower value represents better sustainability performance, the normalization direction was reversed, such that a score of 100% consistently represents the best sustainability performance and 0% represents the worst performance.

Table 1 summarizes the sustainability indicators employed to evaluate the process alternatives from material, energy, environmental, and economic perspectives. The purpose of the framework is to translate process-specific quantities with different units and magnitudes into a consistent sustainability scale. For each indicator, a best target was defined as the condition associated with maximum sustainability performance, whereas a worst-case value represents the least desirable condition considered in the assessment. The calculated process value for each indicator can therefore be positioned between these two limiting cases and expressed on a normalized 0–100% basis. Indicators for which larger values are desirable, such as reaction yield, atom economy, recycled-material fraction, renewable-energy index, rate of return, and turnover ratio, approach 100% as their values move toward the specified best target. Conversely, indicators representing resource consumption, emissions, costs, or waste generation approach 100% as their values decrease toward the specified minimum target.

The framework contains four groups of indicators. The first group evaluates the effectiveness with which raw materials and water are converted into useful products. The second characterizes energy demand, energy recovery, and the degree to which the process effectively utilizes energy resources. The environmental indicators quantify releases, global-warming-related burdens, water use, and wastewater generation. The economic indicators measure utility costs and the ability of the process to generate a financially attractive return over its operating life. In this manner, the framework avoids judging process sustainability using a single efficiency or economic metric and instead considers several complementary aspects of process performance.

The material-sustainability indicators (M1–M14) evaluate how efficiently raw materials and water are utilized within the process. M1–M4 assess the reaction performance through reaction yield, atom economy, actual atom economy, and reaction mass efficiency. M5–M9 quantify the overall material use and losses through total material consumption, mass intensity, value mass intensity, mass productivity, and mass loss index. M10–M11 account for the contribution of recycled and recyclable materials, while M12–M14 evaluate the water consumption in absolute, product-specific, and value-based terms. Together, these indicators describe the efficiency of material conversion, recycling, and water utilization.

The energy-sustainability indicators (E1–E7) characterize both the magnitude and quality of energy use. E1–E3 represent the specific energy intensity, energy intensity

relative to economic value, and waste-treatment energy demand. E4–E6 evaluate the resource energy efficiency, renewability energy index, and process-integration degree, thereby capturing how effectively energy is utilized and recovered within the process. E7, the energy return on investment, provides an overall measure of the useful energy obtained relative to the energy invested.

The environmental-sustainability indicators (EN1–EN8) are based on the process-sustainability indicator taxonomy and data-needs framework of Ruiz-Mercado et al. [7–9], as adapted in the methodological sustainability assessment used in the authors' previous process studies [6,18]. EN1–EN3 address toxic-release-related quantities, EN4 represents an air-hazard measure, EN5–EN6 represent global-warming-related quantities, and EN7–EN8 represent water footprint and wastewater generation. In the present manuscript these indicators are evaluated only within the defined operational/process boundary. They do not include a cradle-to-gate inventory for upstream natural-gas production, methane leakage, electrolyzer manufacturing, stack replacement, or end-of-life treatment.

The economic-sustainability indicators (EC1–EC8) evaluate the financial viability of the process. EC1–EC3 focus on water and energy costs, including total water cost, total energy cost, and specific energy cost. EC4 represents economic potential based on revenues and operating costs, while EC5–EC7 assess profitability and capital effectiveness through the rate of return, payback period, and turnover ratio. Finally, EC8, cumulative cash position, reflects the overall financial value generated over the project lifetime. Together, these indicators provide a comprehensive assessment of process profitability, investment attractiveness, and long-term economic performance.

Table 1. The selected sustainability indicators.

				SUSTAINABILITY VALUE	
	INDICATOR	**FORMULA**	**METRIC**	**Best Target (100%)**	**Worst Case (0%)**
		Material-Sustainability Indicators			
M1	Reaction yield	$\mathrm{RY} = \frac{\text{Mass of product}}{\text{Theoretical mass of product}}$	kg/kg	1	0
M2	Atom economy	$\mathrm{AE, desired\ product} = \frac{(Molecular\ weight\ x\ stoichiometric\ coefficient), desired\ product}{\sum_1^{reagents}(Molecular\ weight\ x\ stoichiometric\ coefficient) reagent}$	kg/kmol/ kg/kmol	1	0
M3	Actual atom economy	$\mathrm{AAE} = \mathrm{AE} \times \mathrm{RY}$	kg/kmol/ kg/kmol	1	0
M4	Reaction mass efficiency	$\mathrm{SF} = \frac{\text{Mass of product}}{\text{Total mass of reagents}}$	kg/kg	1	0
M5	Total material consumption	$\mathrm{M, TOT} = Total\ mass\ input$	kg	Mass of product	40 times mass of product
M6	Mass intensity	$\mathrm{MI} = \frac{\text{Total mass input}}{\text{Mass of product}}$	kg/kg	1	40
M7	Value mass intensity	$\mathrm{MIV} = \frac{\text{Total mass input}}{\text{Sales revenue or value added}}$	kg/$	0	52
M8	Mass productivity	$\mathrm{MP} = \frac{\text{Mass of product}}{\text{Total mass input to process or process step}}$	kg/kg	1	0
M9	Mass loss index	$\mathrm{MLI} = \frac{\text{Total nonproduct mass out of process or process step}}{\text{Mass of product}}$	kg/kg	0	100
M10	Recycled material fraction	$\mathrm{w, recy_mat} = \frac{\text{Recycled mass input}}{\text{Total mass input}}$	kg/kg	1	0
M11	Mass fraction of product from recyclable materials	$\mathrm{w, recy_pro} = \frac{\text{Mass of product from recyclable materials}}{\text{Mass of Product}}$	kg/kg	1	0
M12	Total water consumption	$\mathrm{V} = Volume\ of\ fresh\ water\ consumed\ in\ the\ process\ or\ process\ unit$	m^3/h	0	All fresh water

M13	Fractional water consumption	$\mathrm{FWC} = \frac{\text{Volume of fresh water consumed}}{\text{Mass of Product}}$	m^3/kg	0	2.95
M14	Water intensity	$\mathrm{WI} = \frac{\text{Volume of fresh water consumed}}{\text{Sales revenue or value added}}$	$m^3/\$$	0	1.55 $m^3/\$$
		Energy-Sustainability Indicators			
E1	Specific energy intensity	$\mathrm{R,SEI} = \frac{\text{Net energy used as primary fuel equivalent}}{\text{Mass of product}}$	kj/kg	0	1.949×10^6
E2	Energy intensity	$\mathrm{R,EI} = \frac{\text{Net energy used as primary fuel equivalent}}{\text{Sales revenue or value added}}$	kj/$	0	3.73×10^4
E3	Waste-treatment energy	$\mathrm{WTE} = \frac{\text{Waste treatment energy requirements}}{Mass\ of\ product}$	kj/kg	0	Max $E_{\text{waste treats}}$ per kg
E4	Resource energy efficiency	$\mu = \frac{Energy\ content\ of\ the\ product}{Total\ material - input\ energy}$	kj/kj	0	1
E5	Renewability energy index	$\mathrm{RI,E} = \frac{Net\ energy\ supplied\ from\ renewable\ resources}{Net\ energy\ supplied\ to\ the\ process}$	kj/kj	1	0
E6	Process-integration degree (PID)	$\mathrm{PID} = \frac{Recovered\ energy}{Total\ process\ energy\ demand}$	kj/kj	1	0
E7	Energy return on investment (EROI)	$\mathrm{EROI} = \frac{Energy\ output}{Energy\ input}$	kj/kj	10	0
		Environmental-Sustainability Indicators			
EN1	Specific toxic release	$\mathrm{TRs} = \frac{\text{Total mass of toxics released}}{\text{Mass of product}}$	kg/kg	0	All
EN2	Toxic release intensity	$\mathrm{TR} = \frac{\text{Total mass of toxics released}}{\text{Sales revenue or value added}}$	kg/$	0	All
EN3	Environmental quotient	$\mathrm{EQ} = \frac{\text{Total mass of waste}}{Mass\ of\ product} X\ Unfriendliness\ quotient$	kg/kg	0	All
EN4	Environmental hazard, air hazard	$\mathrm{EH.air} = \frac{\text{Volume of limit concentration air emission equivalents}}{Mass\ of\ product}$	m^3/kg	0	1×10^7
EN5	Global warming potential	$\mathrm{GWP} = \frac{\text{Total mass of CO2 equivalents}}{\text{Mass of product}}$	kg/kg	0- No GWP gas releases	All GWP gas releases
EN6	Global warming intensity	$\mathrm{GWI} = \frac{\text{Total mass of CO2 equivalents}}{\text{Sales revenue or value added}}$	kg/$	0- No GWP gas releases	All GWP gas releases
EN7	Water footprint (WFP)	$\mathrm{WFP} = \frac{\text{Total fresh water used}}{Mass\ of\ product}$	m^3	0	All fresh water
EN8	Wastewater generation rate	$\mathrm{Vi,spec} = \frac{\text{Volume of wastewater generated}}{\text{Mass of product}}$	m^3/kg	0	100
		Economic-Sustainability Indicators			
EC1	Total water cost	Cwater tot. = Absolute cost of water used in the process or process unit	$	0	All water required is provided by fresh water
EC2	Total energy cost	CE, tot. = Absolute cost of energy used	$	1.72×10^{-6}/kJ	1.68×10^{-5}/kJ
EC3	Specific energy costs	$\mathrm{EC,spec} = \frac{\text{Total energy cost}}{\text{Total production cost}}$	$/$	0	≥0.2
EC4	Economic potential	EP = Revenue − Raw material costs − Utility costs	$/kg product	10	0
EC5	Rate of return on investment	$\mathrm{ROI} = \frac{\text{Average annual net profit}}{Fixed\ capital\ investment}$	%/yr	30	0
EC6	Payback period	$\mathrm{PBP} = \frac{\text{Fixed capital investment}}{Average\ annual\ cash\ flow}$	yr	1	Plant life cycle
EC7	Turnover ratio	$\mathrm{TR} = \frac{\text{Gross annual sales}}{Fixed\ capital\ investment}$	$/$	4	0
EC8	Cumulative cash position	CCP = The worth of the project at the end of its life	$	Fixed capital investment	0

The complete indicator-by-indicator results are presented in Supplementary Materials S5–S8. This arrangement enables the main manuscript to remain focused on the

comparative interpretation of the sustainability performance while ensuring that the full calculation procedure remains transparent and reproducible.

4. Results and Discussion

4.1. Composition-Dependent Syngas Productivity and Resource Utilization

The first comparison examines how the product specification itself changes the process performance. Because the total AF power is fixed, increasing the H_2 fraction shifts a larger share of the available energy toward water electrolysis and changes the mass of syngas that can be produced per unit power. The analysis therefore treats syngas productivity, CO_2 demand, water demand, and oxygen generation as coupled composition-dependent outputs rather than as separate sustainability indicators.

For illustration, at $H_2/CO = 1$ in Design 1, equal molar H_2 and CO production is obtained from the PEM and AEM branches. Scaling the single-cell result to the common 437 MW power basis gives the corresponding plant-level syngas and O_2 rates; the same procedure is repeated for each composition and architecture.

Figure 4 illustrates the relationship between electricity-normalized syngas production and the dimensionless H_2/CO molar ratio for the three process configurations evaluated using the adopted technology efficiencies (PEM 75%, AEM 70%, and SOE 85%). A decreasing trend is obtained for all designs because increasing the hydrogen fraction increases the electrical energy required per unit mass of product. Design 1 and Design 3 provide the highest calculated productivities under the selected assumptions, whereas Design 2 gives the lowest. For Design 3, this result reflects the adopted literature-based SOE efficiency. The present model does not include an explicit AF-to-SOE heat-exchanger calculation and therefore does not attribute a quantified portion of the advantage to recovered AF heat.

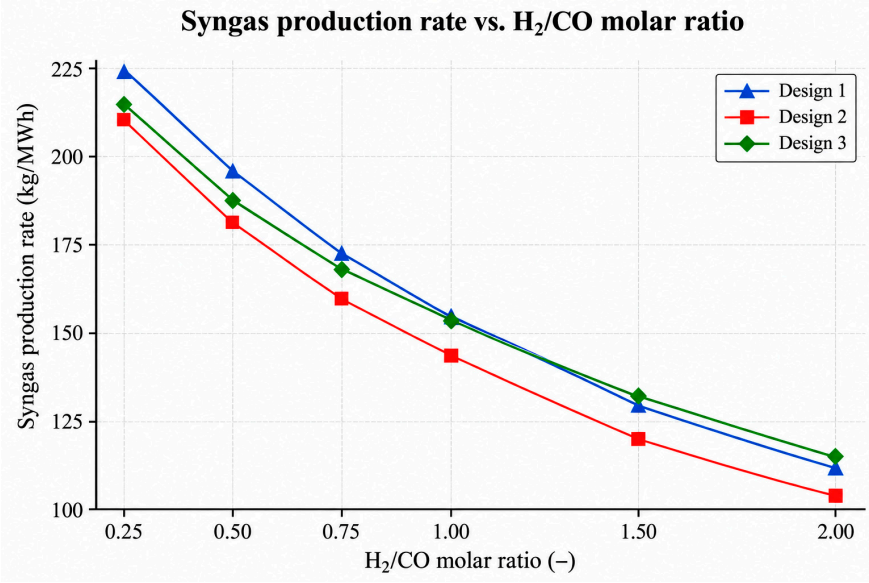


Figure 4. Electricity-normalized syngas-production rate as a function of the dimensionless H_2/CO molar ratio for the three process architectures.

The productivity trends should therefore be interpreted as system-level consequences of the adopted electrolysis efficiencies and product stoichiometry, rather than as experimental performance curves. CO-rich syngas can be relevant to carbonylation chemistry, while oxo-synthesis commonly employs syngas near $H_2/CO \approx 1$ and methanol/DME/Fischer–Tropsch routes generally require more hydrogen-rich feed or upstream ratio adjustment [1–3]. The exact optimum ratio depends on the downstream chemistry

and process configuration. Accordingly, the H_2/CO values in this study define a broad design window rather than a universal specification for each downstream application.

Figure 5 summarizes composition-dependent CO_2/H_2O consumption and O_2 production. A key clarification is that the approximately 5.07×10^6 kg h^{-1} CO_2 value is the large internal circulating sCO_2 stream of the AF loop and must not be described as net CO_2 production. The fresh carbon entering the system originates from the natural-gas feed. On the same AF basis used in the preceding validated model [18], the separated net CO_2-rich product stream is approximately 2.03×10^5 kg h^{-1}, whereas the multi-million-kilogram-per-hour stream is predominantly recycle working fluid. The syngas section diverts approximately 6.31×10^4–1.52×10^5 kg CO_2 h^{-1} depending on architecture and H_2/CO ratio. Thus, the diverted carbon is a fraction of the net CO_2-rich product available from the AF block, while the balance remains available for recycle management and/or export to storage/utilization. This distinction prevents the recycle inventory from being interpreted as newly generated carbon and makes the carbon accounting consistent with the closed-loop function of the AF cycle.

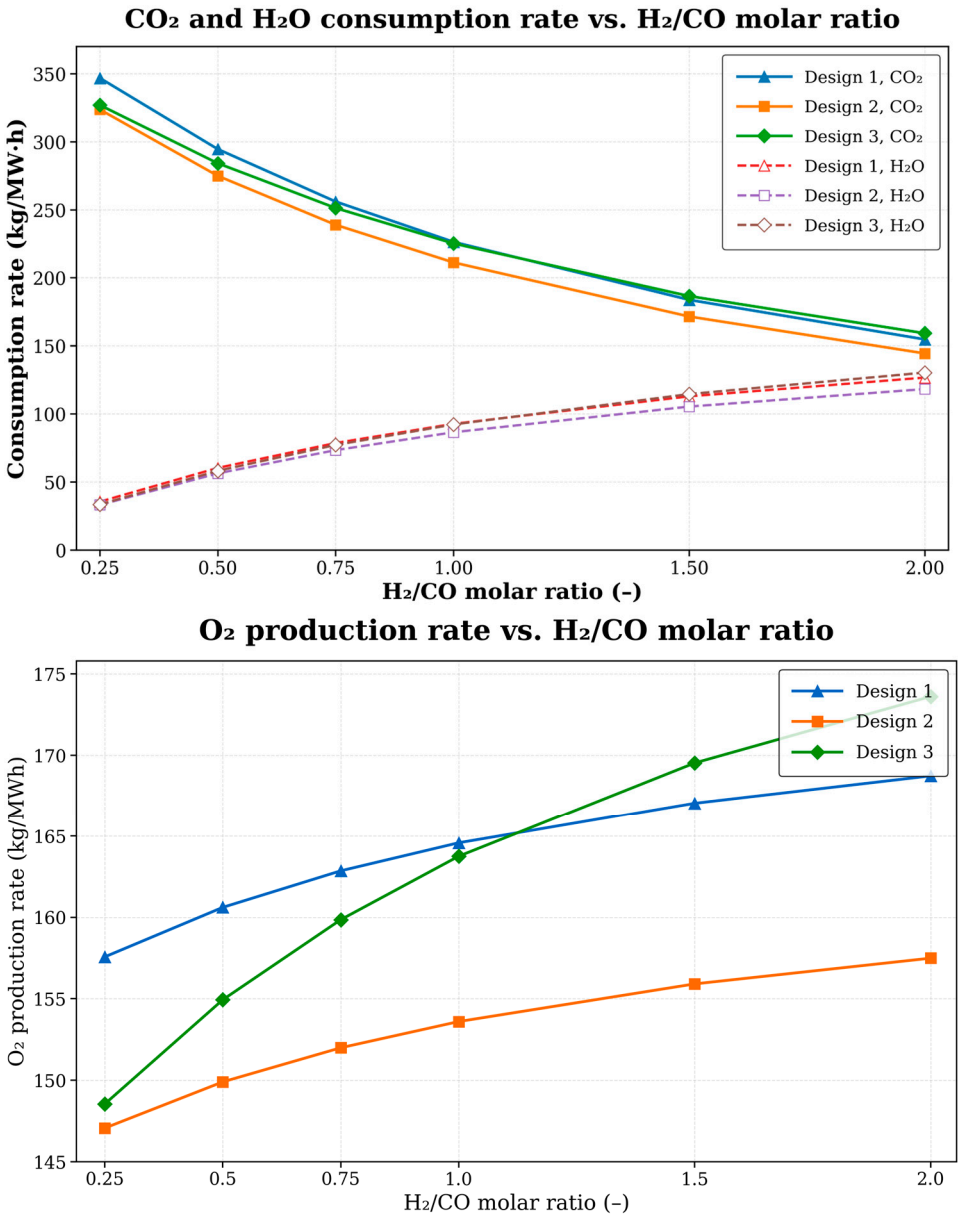


Figure 5. Composition-dependent CO_2/H_2O consumption and O_2 production for the three process architectures.

The calculated electrolysis water demand is approximately 14,472–56,951 kg h^{-1}, compared with about 163,571 kg h^{-1} of recovered AF process water. These values show that the stoichiometric process-water requirement of the electrolysis reactions can be supplied by the recovered AF stream under the modeled steady-state boundary. This result should not be interpreted as zero total external water demand for a complete industrial plant. Water purification/polishing losses, cooling-tower makeup, blowdown, cleaning, stack conditioning, wastewater handling, storage losses, and purge requirements are not quantified in the present model and would create additional make-up demand in practice. The revised manuscript therefore uses the term process-water self-sufficiency rather than claiming complete plant-wide water independence.

Electrolyzer O_2 generation increases with H_2/CO ratio and corresponds to approximately 64,266–75,871 kg O_2 h^{-1}, compared with the AF oxy-combustion requirement of 288,000 kg O_2 h^{-1}. This is equivalent to approximately 22.9–26% of the oxygen requirement. In the present comparison, this quantity is treated as a potential oxygen-supply offset and economic/material integration benefit. The 437 MW electrolysis power basis is not increased by an additional ASU-power saving; therefore, oxygen recycling does not create a second electrical credit in the production calculations. A fully coupled future model should recalculate the ASU power, oxygen compression, electrolysis auxiliaries, gas separation, and product compression simultaneously to quantify the true net power benefit of oxygen integration.

Figure 6 shows that average material sustainability is high for all three designs (≈88.5–92%). For each design, increasing the H_2/CO ratio from 0.25 to 2.0 causes a gradual decrease of about 1–1.3 percentage points in the material sustainability score. This trend indicates that the mass of useful product per unit material input decreases slightly at high H_2/CO ratios. Design 3 consistently exhibits the highest material sustainability (~91.4–92.0%) over the entire H_2/CO range. The high electrolysis efficiency at elevated temperature allows a larger fraction of the CO_2 and H_2O feed to be converted into syngas, minimizing unreacted species, separation duties, and waste streams. Design 1 occupies an intermediate position, while Design 2 shows the lowest material sustainability (~88.7–89.8%), reflecting higher specific material consumption and more by-product or recycle flows for the same syngas output.

More broadly, the consistently high material-sustainability scores demonstrate an important advantage of the proposed integrated AF–electrolysis–syngas system: most of the material entering the process is effectively directed toward useful products rather than being lost through waste or inefficient material circulation. The integration of power generation, electrolysis, and downstream syngas production promotes more efficient use of carbon- and water-containing feedstocks and reduces the need for excessive fresh-material input. Moreover, the relatively narrow variation in material sustainability among the three designs indicates that the integrated process architecture itself provides inherently strong material-utilization performance, while the choice of electrolyzer mainly determines the extent of additional improvement. In particular, Design 3 demonstrates that enhanced electrolysis performance can further increase resource utilization without requiring a fundamentally different process structure. Thus, the proposed system advances material sustainability by combining high feedstock utilization, reduced material losses, lower recycle and waste generation, and improved conversion of CO_2 and H_2O into valuable syngas, supporting a more resource-efficient pathway for low-carbon chemical and fuel production.

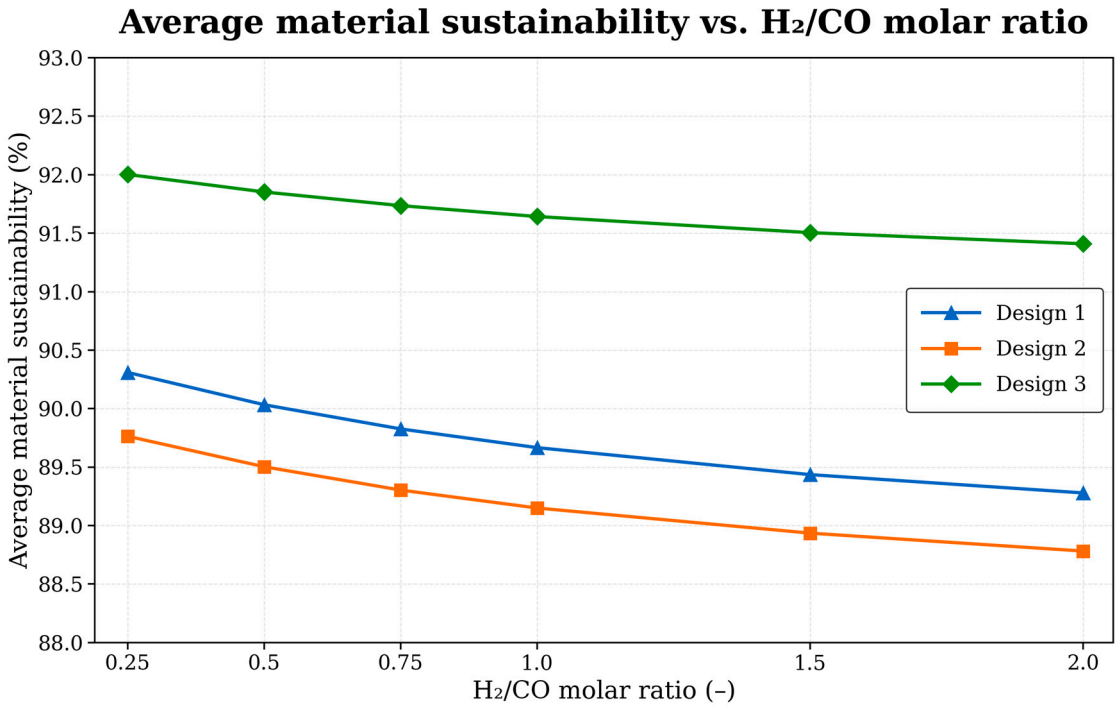


Figure 6. Material-sustainability scores across the H_2/CO composition window. Material-sustainability indicators: M1, reaction yield; M2, atom economy; M3, actual atom economy; M4, reaction mass efficiency; M5, total material consumption; M6, mass intensity; M7, value mass intensity; M8, mass productivity; M9, mass loss index; M10, recycled material fraction; M11, mass fraction of product from recyclable materials; M12, total water consumption; M13, fractional water consumption; M14, water intensity.

4.2. Energy Sustainability Across the Composition Window

Energy sustainability is a critical indicator for evaluating how effectively the integrated process converts supplied electrical and thermal energy into useful chemical energy stored in the syngas product. In the present system, this performance is influenced not only by the electrolyzer efficiency but also by the interaction between the Allam–Fetvedt power cycle, heat integration, electrolysis technology, and the resulting H_2/CO product composition. A higher energy-sustainability score therefore indicates that a larger fraction of the total energy supplied to the overall process is retained in the desired syngas product, with lower relative losses through conversion inefficiencies, auxiliary power consumption, and intermediate conditioning requirements. Because PEM, AEM, and SOE differ substantially in their electrical and thermal energy requirements, the selected electrolyzer technology has a direct influence on the overall energy performance of the integrated system.

Figure 7 reports a composite energy-sustainability score, not an individual energy indicator. Each E1–E7 indicator is first normalized separately to the common 0–100% sustainability scale using the best/worst references in Table 1, after which the seven normalized values are given equal weight and averaged arithmetically. This procedure prevents indicators with larger physical units from numerically dominating the composite score. Under this method, the average score increases modestly with H_2/CO ratio for all three designs; however, the magnitude and ranking should be interpreted as method-dependent screening results rather than absolute thermodynamic efficiencies.

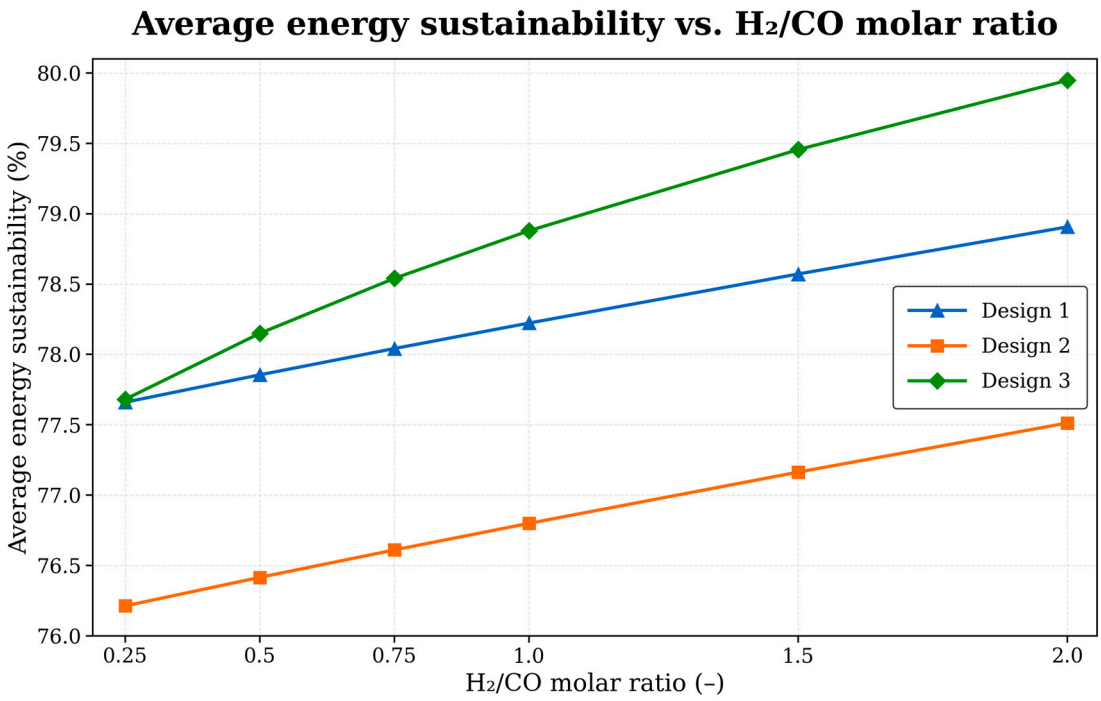


Figure 7. Equal-weight average energy-sustainability scores as a function of the dimensionless H_2/CO molar ratio for the three designs. The composite score is the arithmetic mean of the individually normalized E1–E7 indicators: E1, specific energy intensity; E2, energy intensity; E3, waste-treatment energy; E4, resource energy efficiency; E5, renewability energy index; E6, process-integration degree (PID); E7, energy return on investment (EROI).

Design 3 gives the highest composite energy-sustainability score through most of the investigated range under the adopted 85% SOE process-efficiency assumption. High-temperature electrolysis can, in principle, shift part of the splitting-energy requirement from electricity to heat and can therefore offer attractive integration opportunities with hot process streams. In the present study, however, the SOE heat duty and an AF-to-SOE heat exchanger are not explicitly simulated. The observed advantage should therefore be attributed to the adopted literature-based SOE efficiency and the resulting process-level energy balance, not to a quantified heat-recovery duty from the AF cycle.

The increasing separation between Design 3 and the lower-temperature routes at hydrogen-rich compositions therefore indicates sensitivity to the assumed technology efficiency rather than proof of a specific AF heat-integration design. Future work should quantify the SOE steam-generation duty, available AF heat-source temperature levels, exchanger minimum approach temperature, pressure losses, and the effect of heat extraction on AF net power before a numerical heat-integration credit is assigned.

Design 1 shows intermediate performance over the full composition range. With a PEM efficiency of 75%, its electrical-energy requirement is lower than that of Design 2 but higher than that of Design 3. Accordingly, its energy-sustainability score remains consistently between those of the AEM- and SOE-based systems. The nearly linear increase with H_2/CO ratio indicates that the energetic benefit of increasing hydrogen content is maintained across the investigated range without a sharp deterioration in auxiliary-energy requirements.

Design 2 remains the least energy-sustainable configuration, increasing only from approximately 76.2% to 77.5%. This lower performance is primarily associated with the lower assumed AEM efficiency of 70%, which requires a greater electrical input for producing the same amount of hydrogen. As a result, a smaller fraction of the energy supplied to the integrated AF–electrolyzer system is retained in the final syngas product.

Although increasing the H_2/CO ratio still improves the score, the benefit is partially offset by the higher specific electricity demand of the AEM unit.

From a system-integration perspective, the results also demonstrate that energy sustainability is governed by more than the nominal efficiency of the electrolyzer alone. The extent to which thermal energy can be recovered internally, the amount of auxiliary power required for gas conditioning and separation, and the level of integration between the power block and electrolysis section all influence the final score. The superior performance of Design 3 therefore reflects both the intrinsic efficiency of SOE and its stronger compatibility with high-temperature heat integration. In this sense, the proposed integrated AF–electrolysis configuration advances energy sustainability by simultaneously converting low-carbon electricity and recoverable process heat into a storable chemical-energy carrier.

4.3. Environmental Performance

Environmental sustainability is evaluated here only as a process-level operational screening exercise using EN1–EN8. Because the three configurations share the same AF power block and carbon-management boundary, the normalized scores mainly reflect differences in modeled operational resource use. Upstream natural-gas extraction and processing, methane leakage, electrolyzer and balance-of-plant manufacturing, catalyst/membrane/ceramic production, stack replacement, CO_2 transport/storage infrastructure, recycling, and end-of-life treatment are not included in the calculation. Accordingly, the environmental scores must not be interpreted as cradle-to-gate or cradle-to-grave life-cycle results.

Figure 8 shows closely clustered process-level normalized environmental scores of 99.12% for AF + Design 1, 98.99% for AF + Design 2, and 99.31% for AF + Design 3. These percentages are relative scores generated by the adopted indicator normalization procedure; they are not absolute greenhouse-gas reduction percentages, and they do not represent a quantified life-cycle carbon intensity. Because the present model does not contain a methane-leakage assumption or a complete upstream life-cycle inventory, an absolute kg CO_2-eq per kg syngas value is not reported. Adding such a value without a defensible life-cycle dataset would overstate the scope of the analysis.

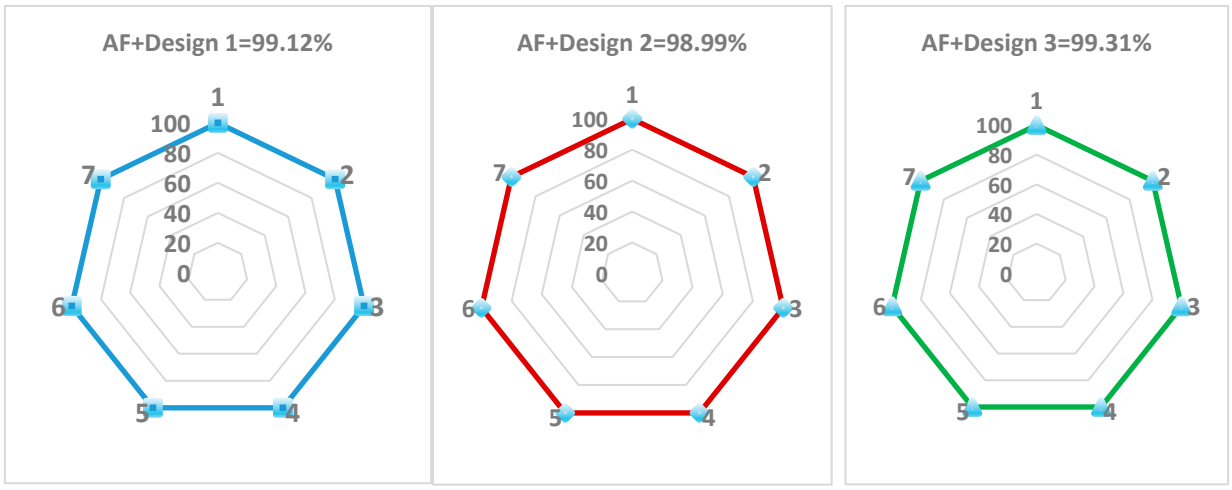


Figure 8. Environmental-sustainability indicators for the three AF-integrated syngas architectures. Environmental-sustainability indicators: EN1, specific toxic release; EN2, toxic release intensity; EN3, environmental quotient; EN4, environmental hazard/air hazard; EN5, global warming potential; EN6, global warming intensity; EN7, water footprint (WFP); EN8, wastewater generation rate.

The limited sensitivity of environmental performance to the H_2/CO ratio can be explained by the intrinsic architecture of the proposed integrated process. Changes in syngas composition mainly redistribute the relative production of H_2 and CO within an otherwise common system rather than introducing fundamentally different feedstocks, combustion routes, or emission-intensive unit operations. The AF cycle continues to provide a concentrated CO_2 stream suitable for capture, while water and carbon-containing streams remain internally integrated with the electrolysis and syngas-production sections. Consequently, the principal sources of environmental burden remain largely unchanged when the H_2/CO ratio is varied. The composition window therefore has a stronger influence on energy requirements and product distribution than on the environmental indicators themselves.

This behavior also explains why the differences among AF + Design 1, AF + Design 2, and AF + Design 3 are comparatively small. All three designs benefit from the same fundamental environmental advantages of the proposed system: very high CO_2 capture, limited direct atmospheric emissions, internal resource integration, and conversion of captured carbon and water into useful products. The electrolyzer type modifies electricity consumption, thermal integration, and equipment-related material requirements, but these differences are relatively small compared with the common environmental benefits provided by the integrated AF process. As a result, the choice of electrolyzer does not produce the same degree of differentiation in environmental sustainability that is observed in the energy or economic dimensions.

AF + Design 3 nevertheless provides the highest average environmental sustainability score. Its superior electrolysis efficiency reduces the specific energy requirement for syngas production and therefore slightly lowers the environmental burden associated with electricity generation and auxiliary operation. The high-temperature integration available in Design 3 also enables greater utilization of internally available process heat, further reducing the need for additional external energy input. AF + Design 1 follows closely, while AF + Design 2 has the lowest score, although the difference is only marginal. This confirms that all three configurations already operate within a high environmental-sustainability region, and the relative ranking should therefore not be interpreted as representing a major environmental disadvantage for any individual design.

Another important feature of the proposed system is the substantial reduction in direct operational emissions. In a conventional natural-gas-fired process, carbon leaves the system primarily through the exhaust gas, whereas the Allam–Fetvedt cycle produces a high-pressure CO_2-rich stream that can be captured with substantially reduced reliance on conventional post-combustion separation. Integrating this power cycle with electrolysis and syngas production further allows electricity, heat, CO_2, and water streams to be utilized across the overall process rather than treated as isolated inputs or wastes. This process integration helps explain the consistently high values obtained for the selected environmental indicators.

Potential upstream and life-cycle burdens remain important and could materially alter the ranking. Natural-gas extraction, processing, transmission, and methane leakage would add greenhouse-gas emissions upstream of the AF plant. PEM and AEM systems require polymeric membranes, catalysts, porous transport layers, and repeated stack replacement, while SOE systems require energy-intensive ceramic processing, metallic interconnects, seals, and high-temperature balance-of-plant materials. Mining and refining of critical materials, manufacturing energy, replacement frequency, recycling yield, and end-of-life treatment can therefore produce environmental burdens that are not visible in the present operational scores. These effects should be quantified in a dedicated cradle-to-gate or cradle-to-grave LCA using explicit methane-leakage and CO_2-storage assumptions.

Taken together, Figure 8 should therefore be interpreted as evidence that the three alternatives have similar environmental performance within the selected operational indicator framework, not as proof of near-zero life-cycle impact. The strongest conclusion supported by the present model is that direct process CO_2 release is strongly constrained by the AF capture/recycle architecture and that the three syngas routes differ only modestly in the normalized operational environmental indicators. Broader environmental claims require an independent life-cycle assessment.

The small environmental-performance differences among the three designs further indicate that technology selection is unlikely to be governed by environmental efficiency alone under the present system boundary. Instead, once all configurations have reached this high environmental-sustainability regime, factors such as energy efficiency, CAPEX and OPEX, electrolyzer durability, stack replacement frequency, operational flexibility, and critical-material requirements become increasingly important for distinguishing among the alternatives. In this respect, the environmental results complement the other sustainability dimensions by showing that the proposed integrated process maintains strong environmental performance while allowing the final technology choice to be guided by broader techno-economic and operational considerations.

4.4. Economic Operating Windows

The economic analysis is used to identify scenario-dependent operating windows rather than to imply a universal market profitability. The calculation uses a 25-year project horizon and a 10% discount rate, consistent with the preceding AF techno-economic framework [18]. The common AF economic basis adopts a natural-gas price of 2.93 USD $MMBtu^{-1}$ and values oxygen as an avoided external-supply cost within the system boundary, consistent with the preceding study [18]. Because no single market price exists for syngas across H_2/CO ratios, product revenue is scenario dependent and the profitability results should be read as model-based operating windows. A configuration is classified as economically feasible only when NPV at the adopted 10% discount rate is non-negative over the 25-year project horizon and the corresponding ROI is positive; cases only marginally above zero are treated as boundary cases rather than robustly profitable designs. Detailed AF costing, technology-specific CAPEX/OPEX ranges, and indicator formulas are reported in Supplementary Section S8. Table 2 retains only the plant-level cost ranges needed to interpret the cash-flow results in the main text.

Table 2. Plant-level CAPEX and fixed-OPEX ranges adopted for the three syngas architectures.

Design	CAPEX [M$]		Fixed OPEX [M$]		Replacement Costs for 25 Years of Plant Life [M$]	
	High	Low	High	Low	High	Low
1	553.22	236.78	20.47	8.96	304.27	130.23
2	437	218.5	13.11	4.31	240.35	120.17
3	1966.5	874	98.32	43.7	1081.57	480.7

Figure 9 presents cumulative cash-flow trajectories under the optimistic cost scenario. Economic feasibility is now defined consistently as NPV ≥ 0 at the 10% discount rate over the 25-year project horizon together with positive ROI. Cases that fail either condition are classified as economically infeasible. Cases that are only slightly above the threshold are identified as marginal rather than grouped with robustly profitable designs. Under this criterion, the strongest positive-return cases occur for the low-temperature architectures at H_2/CO = 1.5–2.0. The Design 3 case at H_2/CO = 2 lies close to the feasibility boundary and is therefore described as marginal, not as a clearly profitable case. This revised

terminology removes the apparent inconsistency between the cash-flow discussion and the later sustainability comparison.

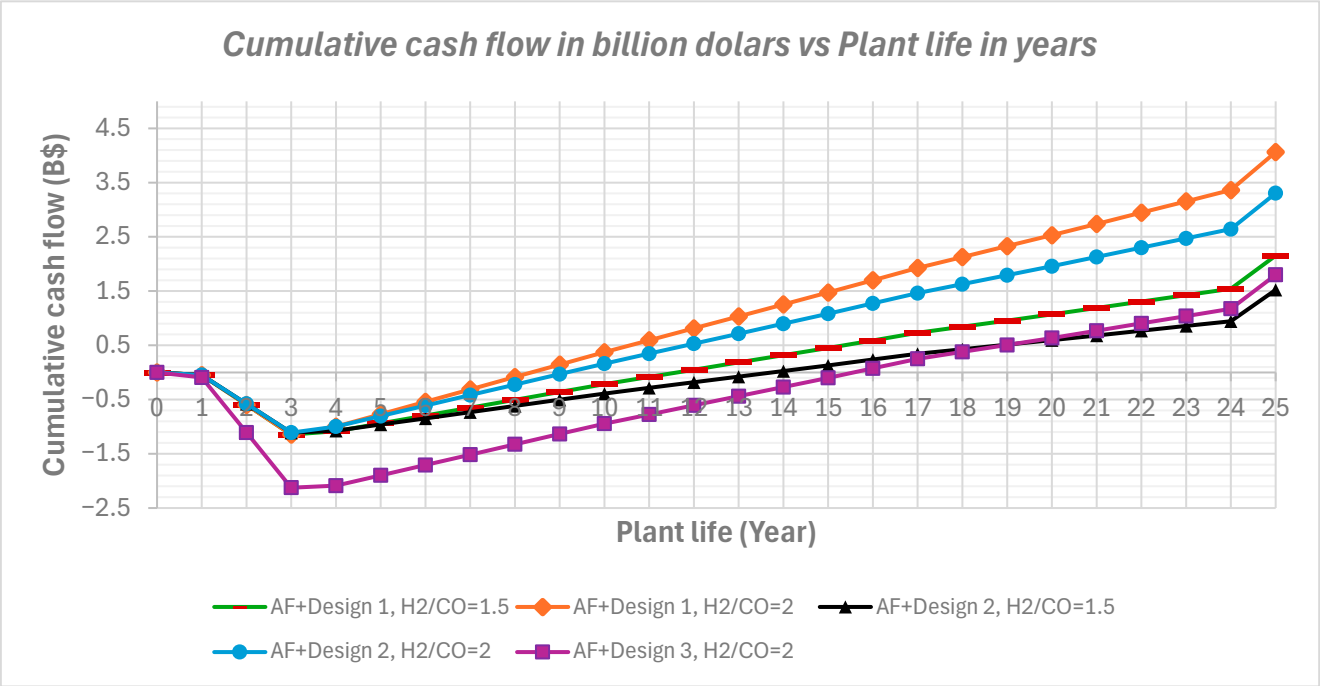


Figure 9. Cumulative cash flow over the plant life for the three process architectures under optimistic CAPEX/OPEX assumptions.

Consequently, these negative-return cases are not displayed in Figure 9 to avoid obscuring the economically relevant trends. CCF(t) tracks how the project's cash balance develops over the 25-year lifetime without discounting. The year when CCF(t) first becomes ≥ 0 gives the simple payback period. Among all evaluated configurations, only a limited subset of Allam–Fetvedt (AF)–integrated cases, specifically higher H_2/CO ratios of 1.5 and 2.0 AF + Design 1 with H2/CO = 1.5, AF + Design 1 with H_2/CO = 2, AF + Design 2 with H_2/CO = 1.5, AF + Design 2 with H_2/CO = 2, and AF + Design 3 with H_2/CO = 2) achieves a positive rate of return on investment (ROI). However, the AF + Design 3 case at H_2/CO = 2 lies very close to the adopted economic feasibility boundary and is therefore classified as a marginal or boundary case rather than as a robustly profitable configuration. Its economic classification is particularly sensitive to the assumed capital cost, stack-replacement cost, utilization factor, product value, and treatment of the oxygen co-product. Accordingly, this case is discussed separately from the clearly positive-return configurations and should not be interpreted as demonstrating robust economic feasibility. In contrast, scenarios with lower H_2/CO ratios systematically yield negative ROI under the current techno-economic assumptions. This trend indicates that not only the total syngas production, but also its composition, plays a decisive role in determining the profitability of the integrated power-to-syngas system.

From an energy and process-integration standpoint, syngas with a low H_2/CO ratio carries a less favorable distribution of chemical energy for the targeted downstream pathways. For the remaining, non-profitable configurations (particularly those at lower H_2/CO), reaching economic feasibility would require substantial improvements on both cost and performance. First, a significant reduction in the electrolyzer system CAPEX is needed to reduce the capital intensity of syngas production when the product has a lower hydrogen content and hence, a lower unit value. Second, improvements in overall energy efficiency (e.g., lower specific electricity consumption via better electrolyzer performance

and tighter heat integration with the AF cycle) would directly reduce variable OPEX. In parallel, lower low-carbon electricity prices, higher operating capacity factors, and potential policy instruments (e.g., carbon pricing, green fuel premiums, or investment incentives) could further improve the economics. In combination, such measures could shift currently unprofitable low-H_2/CO cases toward marginal or positive ROI, expanding the economically viable operating window of the integrated AF–electrolyzer system.

For the best case of each design, AF + Design 1 with H_2/CO = 2 configuration recovers its initial investment fastest, with payback occurring roughly at 6.5 years (considering that the facility does not run for the first three years) and AF + Design 2 with H_2/CO = 2 option follows, achieving payback around year 7.8. The analysis highlights that the rate of return on investment (ROI) values was calculated as 17% (AF + Design 1 with H_2/CO = 2) and 14% (AF + Design 2 with H_2/CO = 2).

Figure 10 presents discounted cash flow and cumulative discounted cash flow for the leading cases under the same optimistic assumptions. The figure should not be interpreted as showing that all three architectures are robustly economically viable. Designs 1 and 2 provide the clearest positive-return cases in the adopted scenario, whereas Design 3 remains a boundary case because its high capital and replacement costs erode the benefit of its higher nominal efficiency. The economic conclusions are therefore conditional on the stated discount rate, utilization factor, product-valuation assumptions, natural-gas price, oxygen treatment, and cost scenario.

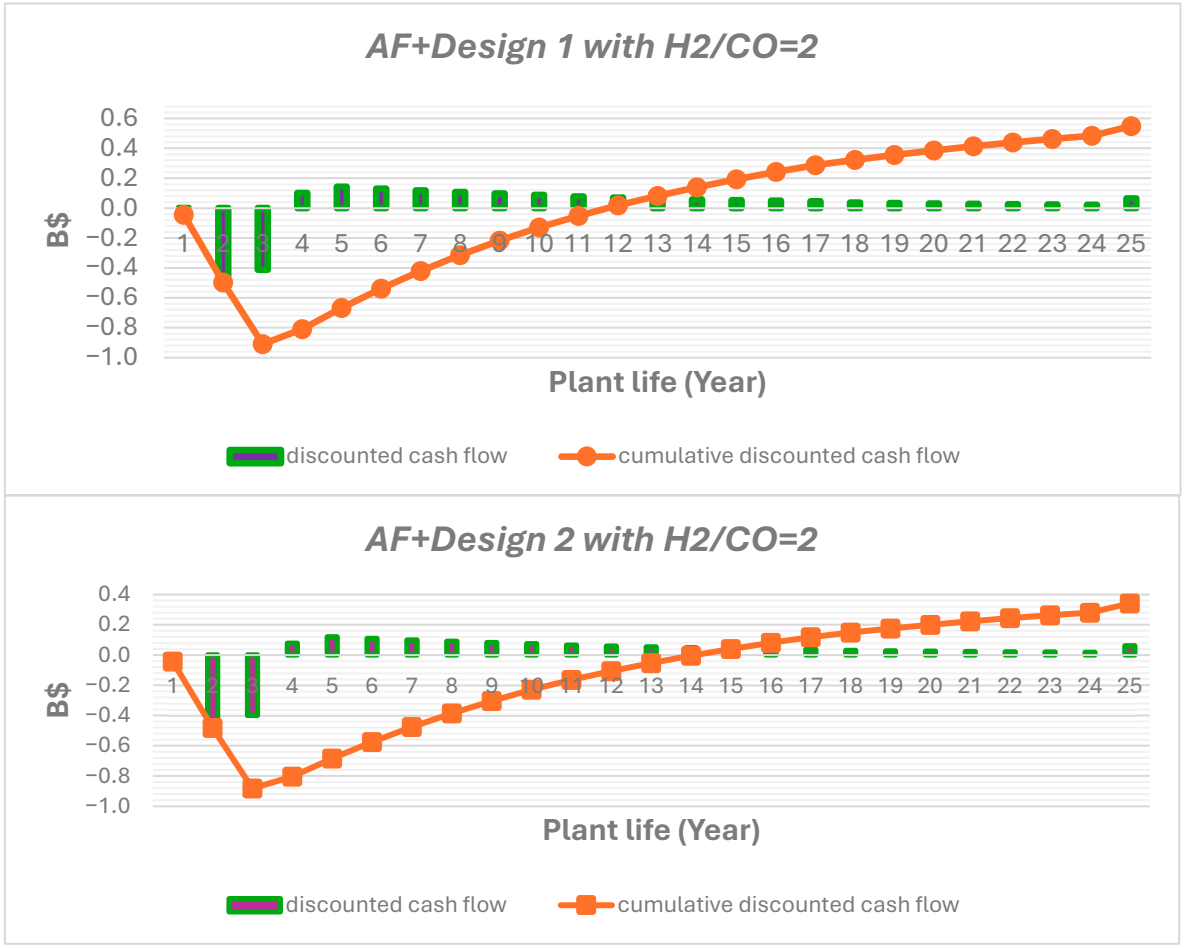


Figure 10. Discounted and cumulative discounted cash flows for the leading positive-return cases.

Figure 11 compares the equal-weight average economic-sustainability scores for the AF-integrated cases that approach or achieve positive ROI at H_2/CO ratios of 1.5–2.0. Each EC1–EC8 indicator is normalized individually and then averaged with equal weights; the

plotted value is therefore a composite economic-sustainability index rather than an energy-sustainability score. AF + Design 1 at $H_2/CO = 2$ gives the highest composite score (≈69%) among the displayed cases. The result reflects the combined effects of product valuation, capital intensity, operating costs, ROI, payback, turnover, and cumulative cash position within the adopted scenario.

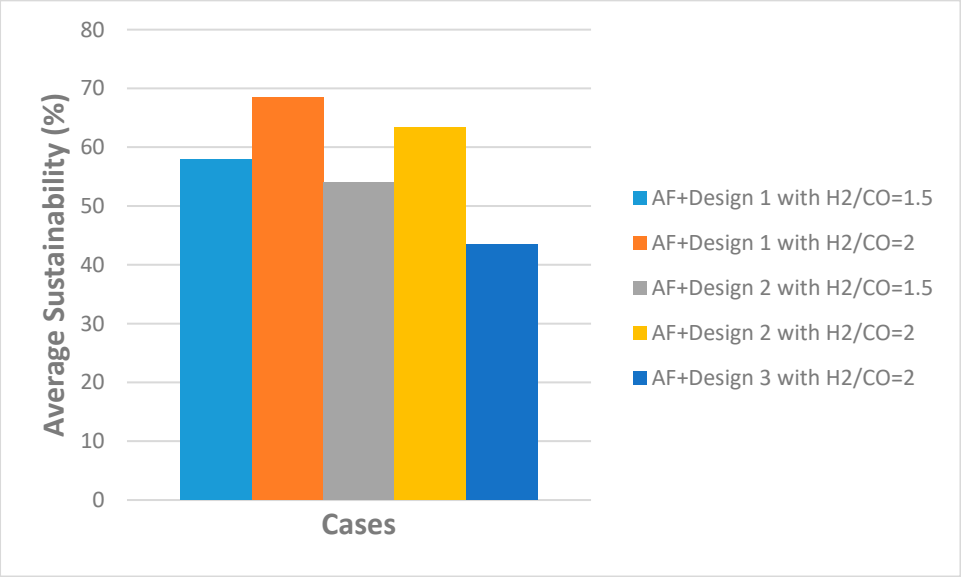


Figure 11. Equal-weight economic-sustainability scores for cases that approach or achieve positive economic returns. Economic-sustainability indicators: EC1, total water cost; EC2, total energy cost; EC3, specific energy costs; EC4, economic potential; EC5, rate of return on investment; EC6, payback period; EC7, turnover ratio; EC8, cumulative cash position.

AF + Design 3 at $H_2/CO = 2$ has the lowest economic-sustainability score (≈43%) despite the higher nominal SOE efficiency. This is consistent with its high CAPEX and replacement burdens. Because its economic return lies close to the feasibility threshold, the revised manuscript treats this case as marginal rather than economically feasible in a robust sense. The result also reinforces that the current model does not quantify an AF-to-SOE heat-integration credit; future reductions in SOE cost or a separately validated heat-integration benefit could shift this boundary.

An important limitation of the present techno-economic assessment is that a formal multi-parameter sensitivity or uncertainty analysis has not been performed. The profitability boundaries reported here should therefore be interpreted as scenario-specific screening results rather than robust break-even thresholds. Among the principal parameters, higher syngas product value and higher plant utilization would be expected to improve NPV and ROI by increasing revenue and improving capital utilization, whereas higher natural-gas prices would increase the effective cost of the AF-based energy supply and reduce the economic margin. The electrolyzer stack lifetime also has a direct influence through the replacement expenditure; a longer stack life would reduce life-cycle costs, whereas more frequent replacement would penalize, especially with the capital-intensive configurations. In addition, the oxygen co-product is presently valued as an avoided external-supply cost. Reducing or eliminating this oxygen credit would therefore decrease the economic attractiveness of all configurations. Because these parameters can shift the location of the feasibility boundary, the specific H_2/CO operating windows identified in this study should not be interpreted as universally valid economic limits. Dedicated sensitivity and uncertainty analyses varying the product value, natural-gas price, capacity

factor, stack lifetime, oxygen credit, and major CAPEX/OPEX assumptions are therefore required before industrial investment conclusions can be drawn.

5. Conclusions

This work reframed AF-integrated electrolysis as a composition-tunable syngas-design problem. Three architectures—separate PEM + AEM production with blending, AEM co-electrolysis, and solid-oxide co-electrolysis—were compared on the same 437 MW-net AF power basis while the product H_2/CO ratio was varied from 0.25 to 2.0. The 437 MW value is retained as a fixed baseline net power constraint; oxygen recycling is not credited as additional electrolysis power. The process model therefore isolates architecture and composition effects while avoiding double counting of the potential ASU benefit.

The resource balances remain favorable at the process level, but their interpretation has been tightened. The approximately 5.07×10^6 kg h^{-1} CO_2 value is an internal circulating sCO_2 flow, not net CO_2 generation. The syngas section uses approximately 6.31×10^4–1.52×10^5 kg CO_2 h^{-1} from the captured product stream, while the stoichiometric electrolysis water demand corresponds to about 8.9–35% of recovered AF process water. The latter supports process-water self-sufficiency under the modeled steady-state boundary, but does not include purification, cooling-tower makeup, purge, cleaning, or other plant-wide water losses. Electrolyzer O_2 is equivalent to roughly 22.9–26% of the AF oxygen demand and is treated as a potential supply offset rather than as an additional electrical credit.

The economic results define a narrower operating region than the technical results. Using the stated 25-year, 10%-discount-rate economic boundary, positive-return cases are concentrated mainly in hydrogen-rich operation for the low-temperature architectures, while the solid-oxide case remains close to the feasibility boundary because of current capital and replacement costs. These conclusions are scenario dependent and should not be generalized beyond the adopted utilization factor, fuel price, oxygen treatment, and product-valuation assumptions.

The principal contribution of the study is therefore the coupled architecture–composition design space rather than a claim of universally optimal or fully renewable syngas production. The sustainability percentages are relative process-level screening scores and not life-cycle GHG intensities. Future work should (i) replace the process-level electrolysis surrogates with electrochemical models or pilot data that resolve faradaic efficiency, voltage, current density, and degradation; (ii) develop a fully coupled electrical balance that includes ASU power, electrolysis auxiliaries, gas separation, and product compression; (iii) quantify SOE heat duty and AF heat-exchanger integration with explicit temperature approaches and net power feedback; (iv) perform cradle-to-gate LCAs that including upstream natural-gas methane leakage, electrolyzer manufacturing and replacement, CO_2 storage, and end-of-life treatment; (v) test alternative sustainability normalization ranges and weighting methods; and (vi) expand the techno-economic sensitivity analysis to the product value, natural-gas price, capacity factor, stack lifetime, and oxygen credit before defining industrial profitability windows.

Supplementary Materials: The following supporting information can be downloaded at: https://www.mdpi.com/article/10.3390/hydrogen7040187/s1, Figure S1: Simplified flowsheet of the Allam–Fetvedt cycle; Figure S2: Allam–Fetvedt cycle simulation; Figure S3: Single-cell simulation of the Design 1; Figure S4: Single-cell simulation of Design 2; Figure S5: Single-cell simulation of Design 3; Table S1: Allam–Fetvedt-cycle unit's main inlet and outlet streams; Table S2: PEM + AEM electrolyzer unit's main inlet and outlet streams for the case of H_2/CO = 1; Table S3: AEM co-electrolyzer unit's main inlet and outlet streams for the case of H_2/CO = 1; Table S4: SOE co-electrolyzer unit's main inlet and outlet streams for the case of H_2/CO = 1; Table S5: The material-efficiency indicators (PEM efficiency is 75%, AEM efficiency is 70%, and SOE efficiency is 85%); Table S6: The

energy indicators (PEM efficiency is 75%, AEM efficiency is 70%, and SOE efficiency is 85%); Table S7: The environmental indicators (PEM efficiency is 75%, AEM efficiency is 70%, and SOE efficiency is 85%); Table S8: CAPEX and OPEX values for the Allam–Fetvedt cycle (437 MW system), as reported in this study; Table S9: CAPEX and OPEX values for PEM, AEM, and SOE electrolyzers, as reported in the literature; Table S10: Economic indicators (PEM efficiency is 75%, AEM efficiency is 70%, and SOE efficiency is 85%) [23–40].

Author Contributions: Conceptualization, S.K.; methodology, S.K. and A.A.; software, A.A.; validation, S.K. and A.A.; formal analysis, S.K. and A.A.; investigation, S.K. and A.A.; resources, S.K.; data curation, S.K. and A.A.; writing—original draft preparation, S.K. and A.A.; writing—review and editing, S.K.; visualization, S.K. and A.A.; supervision, S.K. All authors have read and agreed to the published version of the manuscript.

Funding: This research received no external funding.

Institutional Review Board Statement: Not applicable.

Informed Consent Statement: Not applicable.

Data Availability Statement: The data supporting the findings of this study are included in the original manuscript and the Supplementary Materials. Additional data, including detailed calculations, simulation outputs, and supporting analysis files, are available from the corresponding author upon reasonable request.

Acknowledgments: During the preparation of this manuscript, AI was used only for language editing, grammar correction, sentence restructuring, and improvement of readability and academic clarity. The tool was not used to generate original scientific content, perform data analysis, create results, interpret findings, or make conclusions. All technical content, calculations, simulations, sustainability assessment results, techno-economic analysis, interpretations, and final conclusions were developed, checked, and approved by the authors. The authors take full responsibility for the accuracy, integrity, and originality of the manuscript.

Conflicts of Interest: The authors declare no conflict of interest.

References

1. Caballero, J.J.B.; Zaini, I.N.; Yang, W. Reforming processes for syngas production: A mini-review on the current status, challenges, and prospects for biomass conversion to fuels. *Appl. Energy Combust. Sci.* **2022**, *10*, 100064. https://doi.org/10.1016/j.jaecs.2022.100064.
2. Rashid, R.T.; Chen, Y.; Liu, X.; Alam Chowdhury, F.; Liu, M.; Song, J.; Mi, Z.; Zhou, B. Tunable green syngas generation from CO_2 and H_2O with sunlight as the only energy input. *Proc. Natl. Acad. Sci. USA* **2022**, *119*, e2121174119. https://doi.org/10.1073/pnas.2121174119.
3. Raya-Imbernón, A.; Samu, A.A.; Barwe, S.; Cusati, G.; Fődi, T.; Hepp, B.M.; Janáky, C. Renewable Syngas Generation via Low-Temperature Electrolysis: Opportunities and Challenges. *ACS Energy Lett.* **2023**, *9*, 288–297. https://doi.org/10.1021/acsenergylett.3c02446.
4. Hernández, S.; Farkhondehfal, M.A.; Sastre, F.; Makkee, M.; Saracco, G.; Russo, N. Syngas production from electrochemical reduction of CO_2: Current status and prospective implementation. *Green Chem.* **2017**, *19*, 2326–2346. https://doi.org/10.1039/c7gc00398f.
5. Foit, S.R.; Vinke, I.C.; de Haart, L.G.J.; Eichel, R. Power-to-Syngas: An Enabling Technology for the Transition of the Energy System? *Angew. Chem. Int. Ed.* **2017**, *56*, 5402–5411. https://doi.org/10.1002/anie.201607552.
6. Karagöz, S. A Methodological Sustainability Assessment to Process Intensification (MSAtoPI) by reactive-separation systems. *Fuel* **2023**, *348*, 128562. https://doi.org/10.1016/j.fuel.2023.128562.
7. Ruiz-Mercado, G.J.; Smith, R.L.; Gonzalez, M.A. Sustainability Indicators for Chemical Processes: I. Taxonomy. *Ind. Eng. Chem. Res.* **2012**, *51*, 2309–2328. https://doi.org/10.1021/ie102116e.
8. Ruiz-Mercado, G.J.; Smith, R.L.; Gonzalez, M.A. Sustainability Indicators for Chemical Processes: II. Data Needs. *Ind. Eng. Chem. Res.* **2012**, *51*, 2329–2353. https://doi.org/10.1021/ie200755k.

9. Ruiz-Mercado, G.J.; Gonzalez, M.A.; Smith, R.L. Sustainability Indicators for Chemical Processes: III. Biodiesel Case Study. *Ind. Eng. Chem. Res.* **2013**, *52*, 6747–6760. https://doi.org/10.1021/ie302804x.
10. Samu, A.A.; Kormányos, A.; Kecsenovity, E.; Szilágyi, N.; Endrődi, B.; Janáky, C. Intermittent Operation of CO_2 Electrolyzers at Industrially Relevant Current Densities. *ACS Energy Lett.* **2022**, *7*, 1859–1861. https://doi.org/10.1021/acsenergylett.2c00923.
11. Abousalmia, A.; Karagoz, S. Design and Simulation of an Integrated Process for the Co-Production of Power, Hydrogen, and DME by Using an Electrolyzer's System. *Energies* **2025**, *18*, 2446. https://doi.org/10.3390/en18102446.
12. Abousalmia, A.; Al-Remaihi, L.; Al-Kaabi, S.; Jassim, F.; Karagoz, S. Simulation and Environmental Sustainability Assessment of an Integrated LNG-Power Cycle-Electrolyzer-Methanol Process for Clean Energy Generation. *Processes* **2025**, *13*, 1476. https://doi.org/10.3390/pr13051476.
13. Chan, W.; Morosuk, T.; Li, X.; Li, H. Allam cycle: Review of research and development. *Energy Convers. Manag.* **2023**, *294*, 117607. https://doi.org/10.1016/j.enconman.2023.117607.
14. Gai, S.; Yu, J.; Yu, H.; Eagle, J.; Zhao, H.; Lucas, J.; Doroodchi, E.; Moghtaderi, B. Process simulation of a near-zero-carbon-emission power plant using CO_2 as the renewable energy storage medium. *Int. J. Greenh. Gas Control* **2016**, *47*, 240–249. https://doi.org/10.1016/j.ijggc.2016.02.001.
15. Zhang, Q.; Chen, H.; Li, B.; Pan, P.; Xu, G.; Zhao, Q.; Jiang, X. A novel system integrating water electrolysis and supercritical CO_2 cycle for biomass to methanol. *Appl. Therm. Eng.* **2023**, *225*, 120234. https://doi.org/10.1016/j.applthermaleng.2023.120234.
16. Candelaresi, D.; Spazzafumo, G. Production of Substitute Natural Gas Integrated with Allam Cycle for Power Generation. *Energies* **2023**, *16*, 2162. https://doi.org/10.3390/en16052162.
17. Manente, G.; Rahim, A.; Ficarella, A. Methanol-Fired Allam Cycle: Combining Oxy-Fuel Power Cycles With Synthetic E-Fuels. In Proceedings of the ASME Turbo Expo 2024: Turbomachinery Technical Conference and Exposition, London, UK, 24–28 June 2024.
18. Abousalmia, A.; Karagoz, S. Sustainability and Techno-Economic Analysis of a Power-to-Hydrogen Process Employing Low and High-Temperature Water Electrolysis. *Fuels* **2026**, *7*, 64. https://doi.org/10.3390/fuels7030064.
19. Gan, X.; Fernandez, I.C.; Guo, J.; Wilson, M.; Zhao, Y.; Zhou, B.; Wu, J. When to use what: Methods for weighting and aggregating sustainability indicators. *Ecol. Indic.* **2017**, *81*, 491–502. https://doi.org/10.1016/j.ecolind.2017.05.068.
20. Waas, T.; Hugé, J.; Block, T.; Wright, T.; Benitez-Capistros, F.; Verbruggen, A. Sustainability Assessment and Indicators: Tools in a Decision-Making Strategy for Sustainable Development. *Sustainability* **2014**, *6*, 5512–5534. https://doi.org/10.3390/su6095512.
21. Singh, R. K.; Murty, H. R.; Gupta, S. K.; Dikshit, A. K. An overview of sustainability assessment methodologies. *Ecol. Indic.* **2012**, *15*, 281–299. https://doi.org/10.1016/j.ecolind.2008.05.011.
22. Wulf, C.; Haase, M.; Baumann, M.; Zapp, P. Weighting factor elicitation for sustainability assessment of energy technologies. *Sustain. Energy Fuels* **2023**, *7*, 832–847. https://doi.org/10.1039/d2se01170k.
23. Barba, F.C.; Sánchez, G.M.-D.; Seguí, B.S.; Darabkhani, H.G.; Anthony, E.J. A technical evaluation, performance analysis and risk assessment of multiple novel oxy-turbine power cycles with complete CO_2 capture. *J. Clean. Prod.* **2016**, *133*, 971–985. https://doi.org/10.1016/j.jclepro.2016.05.189.
24. Sifat, N.S.; Haseli, Y. A Critical Review of CO_2 Capture Technologies and Prospects for Clean Power Generation. *Energies* **2019**, *12*, 4143. https://doi.org/10.3390/en12214143.
25. Rogalev, A.; Rogalev, N.; Kindra, V.; Komarov, I.; Zlyvko, O. Research and Development of the Oxy-Fuel Combustion Power Cycles with CO_2 Recirculation. *Energies* **2021**, *14*, 2927. https://doi.org/10.3390/en14102927.
26. Hassan, N.; Jalil, A.; Rajendran, S.; Khusnun, N.; Bahari, M.; Johari, A.; Kamaruddin, M.; Ismail, M. Recent review and evaluation of green hydrogen production via water electrolysis for a sustainable and clean energy society. *Int. J. Hydrogen Energy* **2024**, *52*, 420–441. https://doi.org/10.1016/j.ijhydene.2023.09.068.
27. Wang, J.; Wen, J.; Wang, J.; Yang, B.; Jiang, L. Water electrolyzer operation scheduling for green hydrogen production: A review. *Renew. Sustain. Energy Rev.* **2024**, *203*, 114779. https://doi.org/10.1016/j.rser.2024.114779.
28. Badruzzaman, A.; Karagoz, S.; Eljack, F. Sustainable-green hydrogen production through integrating electrolysis, water treatment and solar energy. *Front. Chem. Eng.* **2025**, *7*, 1526331. https://doi.org/10.3389/fceng.2025.1526331.
29. Carmo, M.; Keeley, G.P.; Holtz, D.; Grube, T.; Robinius, M.; Müller, M.; Stolten, D. PEM water electrolysis: Innovative approaches towards catalyst separation, recovery and recycling. *Int. J. Hydrogen Energy* **2019**, *44*, 3450–3455. https://doi.org/10.1016/j.ijhydene.2018.12.030.
30. Varcoe, J.R.; Atanassov, P.; Dekel, D.R.; Herring, A.M.; Hickner, M.A.; Kohl, P.A.; Kucernak, A.R.; Mustain, W.E.; Nijmeijer, K.; Scott, K.; et al. Anion-exchange membranes in electrochemical energy systems. *Energy Environ. Sci.* **2014**, *7*, 3135–3191. https://doi.org/10.1039/c4ee01303d.

31. NI, M.; Leung, M.; Leung, D. Technological development of hydrogen production by solid oxide electrolyzer cell (SOEC). *Int. J. Hydrogen Energy* **2008**, *33*, 2337–2354. https://doi.org/10.1016/j.ijhydene.2008.02.048.
32. Wang, L.; Chen, M.; Küngas, R.; Lin, T.-E.; Diethelm, S.; Maréchal, F.; Van Herle, J. Power-to-fuels via solid-oxide electrolyzer: Operating window and techno-economics. *Renew. Sustain. Energy Rev.* **2019**, *110*, 174–187. https://doi.org/10.1016/j.rser.2019.04.071.
33. Graves, C.; Ebbesen, S.D.; Mogensen, M.; Lackner, K.S. Sustainable hydrocarbon fuels by recycling CO_2 and H_2O with renewable or nuclear energy. *Renew. Sustain. Energy Rev.* **2011**, *15*, 1–23. https://doi.org/10.1016/j.rser.2010.07.014.
34. Park, S.; Choi, K.; Lee, C.; Kim, S.; Yoo, Y.; Chang, D. Techno-economic analysis of adiabatic four-stage CO_2 methanation process for optimization and evaluation of power-to-gas technology. *Int. J. Hydrogen Energy* **2021**, *46*, 21303–21317. https://doi.org/10.1016/j.ijhydene.2021.04.015.
35. Greiml, M.; Fritz, F.; Kienberger, T. Increasing installable photovoltaic power by implementing power-to-gas as electricity grid relief—A techno-economic assessment. *Energy* **2021**, *235*, 121307. https://doi.org/10.1016/j.energy.2021.121307.
36. Pandey, A.; Kumar, R.R.; B, K.; Laghari, I.A.; Samykano, M.; Kothari, R.; Abusorrah, A.M.; Sharma, K.; Tyagi, V. Utilization of solar energy for wastewater treatment: Challenges and progressive research trends. *J. Environ. Manag.* **2021**, *297*, 113300. https://doi.org/10.1016/j.jenvman.2021.113300.
37. Chen, X.; Pang, Z.; Zhang, M.; Jiang, S.; Feng, J.; Shen, B. Techno-economic study of a 100-MW-class multi-energy vehicle charging/refueling station: Using 100% renewable, liquid hydrogen, and superconductor technologies. *Energy Convers. Manag.* **2022**, *276*, 116463. https://doi.org/10.1016/j.enconman.2022.116463.
38. U.S. Department of Energy. *Hydrogen Program Record [Internet]*; U.S. Department of Energy: Washington, DC, USA, 2024.
39. Gómez, J.; Castro, R. Green Hydrogen Energy Systems: A Review on Their Contribution to a Renewable Energy System. *Energies* **2024**, *17*, 3110. https://doi.org/10.3390/en17133110.
40. Khalil, Y.F. Scoring and Ranking Methods for Evaluating the Techno-Economic Competitiveness of Hydrogen Production Technologies. *Sustainability* **2025**, *17*, 5770. https://doi.org/10.3390/su17135770.

Disclaimer/Publisher's Note: The statements, opinions and data contained in all publications are solely those of the individual author(s) and contributor(s) and not of MDPI and/or the editor(s). MDPI and/or the editor(s) disclaim responsibility for any injury to people or property resulting from any ideas, methods, instructions or products referred to in the content.